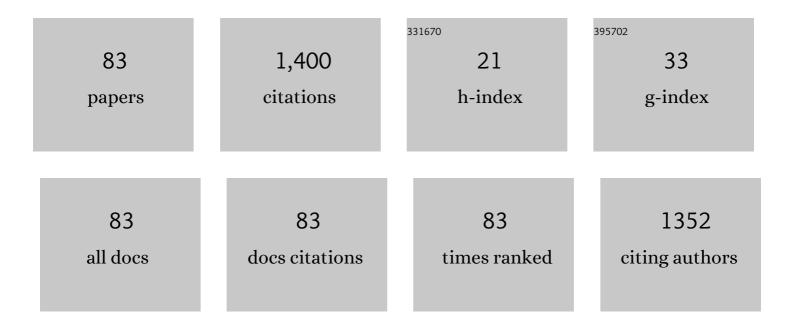
Zong-Bao Wang

List of Publications by Year in descending order

Source: https://exaly.com/author-pdf/5936501/publications.pdf Version: 2024-02-01



#	Article	IF	CITATIONS
1	Nature-Inspired Polyethylenimine-Modified Calcium Alginate Blended Waterborne Polyurethane Graded Functional Materials for Multiple Water Purification. ACS Applied Materials & Interfaces, 2022, 14, 17826-17836.	8.0	7
2	Synthetic Celluloses as Green Fillers for the Enhancement of the Crystallization and Mechanical Properties of Poly(3-hydroxybutyrate- <i>co</i> -3-hydroxyvalerate). ACS Sustainable Chemistry and Engineering, 2022, 10, 6325-6336.	6.7	6
3	Influence of Prereserved Shish Crystals on the Structural Evolution of Ultrahigh-Molecular Weight Polyethylene Films during the Hot Stretching Process. Macromolecules, 2022, 55, 4600-4613.	4.8	11
4	Coupling effects of boron nitride and heat treatment on crystallization, mechanical properties of poly (3-hydroxybutyrate-co-3-hydroxyvalerate) (PHBV). Polymer, 2022, 252, 124967.	3.8	6
5	Structural evolution of UHMWPE gel fibers as high degree plasticized system during stretching: An in-situ wide and small angle X-ray scattering study. Polymer, 2022, 255, 125149.	3.8	7
6	In Situ SAXS and WAXD Investigations of Polyamide 66/Reduced Graphene Oxide Nanocomposites During Uniaxial Deformation. ACS Omega, 2021, 6, 11762-11771.	3.5	7
7	Melting behavior of polymorphic MDI/BD-block TPU investigated by using in-situ SAXS/WAXS and FTIR techniques. Hydrogen bonding formation causing the inhomogeneous melt. Polymer Testing, 2021, 96, 107065.	4.8	13
8	Dramatic toughness improvement of poly(3â€hydroxybutyrateâ€coâ€3â€hydroxyvalerate) by supercritical carbon dioxide–assisted annealing. Polymers for Advanced Technologies, 2021, 32, 3646-3654.	3.2	1
9	The Influence of Ethyl Branch on Formation of Shish-Kebab Crystals in Bimodal Polyethylene under Shear at Low Temperature. Chinese Journal of Polymer Science (English Edition), 2021, 39, 1050-1058.	3.8	4
10	Anisotropically Fatigueâ€Resistant Hydrogels. Advanced Materials, 2021, 33, e2102011.	21.0	114
11	Role of the heat treatment of partial melt recrystallization method on microstructure change and toughness of poly(3-hydroxybutyrate-co-3-hydroxyvalerate) [P(HB-co-HV)]. Polymer, 2021, 228, 123874.	3.8	3
12	Structural Evolution of Polyglycolide and Poly(glycolide- <i>co</i> -lactide) Fibers during the Heat-Setting Process. Biomacromolecules, 2021, 22, 3342-3356.	5.4	6
13	Ultrastretchable, Highly Transparent, Self-Adhesive, and 3D-Printable Ionic Hydrogels for Multimode Tactical Sensing. Chemistry of Materials, 2021, 33, 6731-6742.	6.7	48
14	Shear-induced crystallization of unimodal/bimodal polyethylene at high temperatures affected by C4 short-branching. Polymer, 2021, 233, 124203.	3.8	3
15	Polymorphic microstructure of MDI/BD-block polyurethane as determined by temperature-sensitive conformation variation. Soft Matter, 2021, 17, 9447-9456.	2.7	4
16	Structural Evolution of Polyglycolide and Poly(glycolide <i>-co-</i> lactide) Fibers during In Vitro Degradation with Different Heat-Setting Temperatures. ACS Omega, 2021, 6, 29254-29266.	3.5	6
17	Superhydrophilic Sandwich Structure Aerogel Membrane for Emulsion Separation and Heavy Metal Ion Removal. ACS Applied Polymer Materials, 2021, 3, 5470-5480.	4.4	7
18	Nano-Scale Pores are Formed between the Shish-Kebab Structures of Double-Mold Polyethylene by Supercritical Carbon Dioxide Foaming. Polymer Science - Series A, 2021, 63, 664-671.	1.0	0

ZONG-BAO WANG

#	Article	IF	CITATIONS
19	Formation of well-organized, concentric-ringed spherulites of four-arm star symmetric PEO-b-PCL via confined evaporative crystallization. CrystEngComm, 2020, 22, 7016-7024.	2.6	5
20	Eco-Friendly Strategy to Improve the Processiblity and Properties of Poly(vinyl alcohol) Foams Based on a 3D Hydrogen-Bond Network. Industrial & Engineering Chemistry Research, 2020, 59, 20011-20021.	3.7	4
21	Uniaxial tensile deformation of microinjection molded PCL/SWCNTs nanocomposites: Effect of interfacial "soft epitaxy―on the structural evolution as studied by synchrotron SAXS and WAXD techniques. Polymer, 2020, 198, 122526.	3.8	8
22	Interâ€spherulitic/innerâ€spherulitic localization of PBSU during crystallization of PVDF in PVDF / PBSU blend. Journal of Polymer Science, 2020, 58, 1699-1706.	3.8	11
23	A Synchrotron in situ X-ray Study on the Multiple Melting Behaviors of Isomorphous Poly(3-hydroxybutyrate-co-3-hydroxyvalerate) (P(HB-co-HV)) with Middle HV Content. Chinese Journal of Polymer Science (English Edition), 2020, 38, 1015-1024.	3.8	4
24	Foaming of Poly(3-hydroxybutyrate- <i>co</i> -3-hydroxyvalerate) with Supercritical Carbon Dioxide: Foaming Performance and Crystallization Behavior. ACS Omega, 2020, 5, 9839-9845.	3.5	13
25	Epitaxial Crystallization of Poly(Îμ-caprolactone) on Reduced Graphene Oxide at a Low Shear Rate by <i>In Situ</i> SAXS/WAXD Methods. ACS Omega, 2020, 5, 31535-31542.	3.5	3
26	Understanding of Growth Mechanism and Structure of Multilayer Thin Films via Layer-by-Layer Hydrogen Bonded Assembly from Polymer Brushes-Grafted Surface. Nanoscience and Nanotechnology Letters, 2020, 12, 890-900.	0.4	0
27	The influence of short chain branch on formation of shear-induced crystals in bimodal polyethylene at low shear temperatures. Polymer, 2019, 179, 121625.	3.8	9
28	Structural evolution of stretch deformed HDPE/RGO nanocomposites: An in-situ synchrotron SAXS and WAXD study. Composites Science and Technology, 2019, 183, 107798.	7.8	8
29	Origin of the double melting peaks of poly(3â€hydroxybutyrate―co â€3â€hydroxyvalerate) with a high HV content as revealed by in situ synchrotron WAXD/SAXS analyses. Journal of Polymer Science, Part B: Polymer Physics, 2019, 57, 1453-1461.	2.1	6
30	Effect of Chitin Nanocrystals on the Formation of Shish-Kebab Crystals in Bimodal Polyethylene Injection Bar. Polymer Science - Series A, 2019, 61, 627-634.	1.0	4
31	Microbeam two-dimensional small-angle X-ray scattering investigating the effects of reduced graphene oxide on local microstructures of high-density polyethylene/reduced graphene oxide nanocomposite bars. Royal Society Open Science, 2019, 6, 181866.	2.4	3
32	In-situ investigation of multiple endothermic peaks in isomorphous poly(3-hydroxybutyrate-co-3-hydroxyvalerate) with low HV content by synchrotron radiation. Polymer, 2019, 169, 1-10.	3.8	20
33	Formation and evolution of shishâ€kebab structure during hot stretching in gelâ€spun ultraâ€high molecular weight polyethylene fibers with high concentration gel solution. Polymer Crystallization, 2019, 2, e10060.	0.8	5
34	Effects of a semiâ€bioâ€based triazine derivative on intumescent flameâ€retardant polypropylene. Polymers for Advanced Technologies, 2019, 30, 1259-1268.	3.2	21
35	The Influence of Soft-Epitaxial Crystallization on Polyamide 66/Carbon Nanotubes Composite Injection Bar. Polymer Science - Series A, 2019, 61, 906-912.	1.0	2
36	Effects of shear on epitaxial crystallization of poly(Îμ-caprolactone) on reduced graphene oxide. RSC Advances, 2018, 8, 6406-6413.	3.6	5

ZONG-BAO WANG

#	Article	IF	CITATIONS
37	The influence of short chain branch on formation of shishâ€kebab crystals in bimodal polyethylene under shear at high temperatures. Journal of Polymer Science, Part B: Polymer Physics, 2018, 56, 786-794.	2.1	12
38	The influence of short chain branch on formation of shear induced crystals in bimodal polyethylene at high shear temperatures. European Polymer Journal, 2018, 105, 359-369.	5.4	13
39	Nonbirefringent bands in thin films of a copolymer melt: rapid rhythmic crystal growth with an unusual crystal–melt interface. CrystEngComm, 2018, 20, 2221-2226.	2.6	8
40	Structural transformation from shishâ€kebab crystals to microâ€fibrils through hot stretching process of gelâ€spun ultraâ€high molecular weight polyethylene fibers with high concentration solution. Journal of Polymer Science, Part B: Polymer Physics, 2018, 56, 225-238.	2.1	15
41	Effect of epitaxial crystallization on the structural evolution of PCL/RGO nanocomposites during stretching by in-situ synchrotron radiation. Polymer, 2018, 159, 106-115.	3.8	11
42	The Influence of Space Restriction on the Mechanical Properties of Isotactic Polypropylene/Reduced Graphene Oxide Nanocomposite Injection Bars. Polymer Science - Series A, 2018, 60, 663-670.	1.0	2
43	High-density polyethylene crystals with double melting peaks induced by ultra-high-molecular-weight polyethylene fibre. Royal Society Open Science, 2018, 5, 180394.	2.4	22
44	Epitaxial Crystallization of Precisely Methyl-Substituted Polyethylene Induced by Carbon Nanotubes and Graphene. Crystals, 2018, 8, 168.	2.2	1
45	Structural Effects of Residual Groups of Graphene Oxide on Poly(ε-Caprolactone)/Graphene Oxide Nanocomposite. Crystals, 2018, 8, 270.	2.2	9
46	Structure and properties of gel-spun ultra-high molecular weight polyethylene fibers with high gel solution concentration. Chinese Journal of Polymer Science (English Edition), 2017, 35, 524-533.	3.8	10
47	Strong enhancement of the twisting frequency of achiral orthorhombic lamellae in poly(lµ-caprolactone) banded spherulites via evaporative crystallization. CrystEngComm, 2017, 19, 1210-1219.	2.6	6
48	Structural difference of gel-spun ultra-high molecular weight polyethylene fibers affected by cold drawing process. Fibers and Polymers, 2017, 18, 549-554.	2.1	10
49	Epitaxial crystallization of precisely bromine-substituted polyethylene induced by carbon nanotubes and graphene. RSC Advances, 2017, 7, 17640-17649.	3.6	8
50	The influence of epitaxial crystallization on the mechanical properties of a high density polyethylene/reduced graphene oxide nanocomposite injection bar. RSC Advances, 2017, 7, 21918-21925.	3.6	23
51	Dramatic Toughness Enhancement of Polydicyclopentadiene Composites by Incorporating Low Amounts of Vinyl-Functionalized SiO ₂ . Industrial & Engineering Chemistry Research, 2017, 56, 4750-4757.	3.7	16
52	Structural evolution from shish-kebab to fibrillar crystals during hot-stretching process of gel spinning ultra-high molecular weight polyethylene fibers obtained from low concentration solution. Polymer, 2017, 120, 244-254.	3.8	42
53	Structural development of gel-spinning UHMWPE fibers through industrial hot-drawing process analyzed by small/wide-angle X-ray scattering. Polymer Bulletin, 2017, 74, 721-736.	3.3	19
54	Morphological Control of Polymer Spherulites via Manipulating Radial Lamellar Organization upon Evaporative Crystallization: A Mini Review. Crystals, 2017, 7, 115.	2.2	32

ZONG-BAO WANG

#	Article	IF	CITATIONS
55	The Influence of Epitaxial Crystallization on the Mechanical Properties of Polyamide 66/Reduced Graphene Oxide Nanocomposite Injection Bar. Crystals, 2017, 7, 384.	2.2	14
56	Enhance understanding of rhythmic crystallization in confined evaporating polymer solution films: from environment to solution film and then to one period. RSC Advances, 2016, 6, 45241-45249.	3.6	10
57	Synchronous architecture of ring-banded and non-ring-banded morphology within one spherulite based on in situ ring-opening polymerization of cyclic butylene terephthalate oligomers. RSC Advances, 2016, 6, 94524-94530.	3.6	8
58	The influence of chitin nanocrystals on structural evolution of ultra-high molecular weight polyethylene/chitin nanocrystal fibers in hot-drawing process. Chinese Journal of Polymer Science (English Edition), 2016, 34, 1373-1385.	3.8	9
59	Effect of Gel Solution Concentration on the Structure and Properties of Gel-Spun Ultrahigh Molecular Weight Polyethylene Fibers. Industrial & Engineering Chemistry Research, 2016, 55, 8357-8363.	3.7	22
60	Multiple endothermic peaks resulted from different crystal structures in an isomorphous copolymer poly(3-hydroxybutyrate-co-3-hydroxyvalerate). Chinese Journal of Polymer Science (English Edition), 2016, 34, 1510-1522.	3.8	9
61	Characterization of structural knot distributions in UHMWPE fibers. Chinese Journal of Polymer Science (English Edition), 2016, 34, 606-615.	3.8	5
62	An in situ small-angle X-ray scattering study of the structural effects of temperature and draw ratio of the hot-drawing process on ultra-high molecular weight polyethylene fibers. RSC Advances, 2016, 6, 51125-51134.	3.6	26
63	Ultra-strong gel-spun ultra-high molecular weight polyethylene fibers filled with chitin nanocrystals. RSC Advances, 2016, 6, 20629-20636.	3.6	19
64	Correlation between polymerization of cyclic butylene terephthalate (CBT) and crystallization of polymerized CBT. Chinese Journal of Polymer Science (English Edition), 2015, 33, 1104-1113.	3.8	4
65	Tremor dependant nonlinear interaction in deep brain local field potentials of Parkinson's disease. , 2014, , .		1
66	Reduced graphene oxide enhances the crystallization and orientation of poly(ε-caprolactone). Composites Science and Technology, 2014, 96, 63-70.	7.8	42
67	Morphology of Poly(Ethylene Oxide)- b-Poly(ϵ-Caprolactone) Spherulites Formed Under Compressed CO2. Journal of Macromolecular Science - Physics, 2014, 53, 1137-1144.	1.0	5
68	Tuning Radial Lamellar Packing and Orientation into Diverse Ring-Banded Spherulites: Effects of Structural Feature and Crystallization Condition. Macromolecules, 2014, 47, 1783-1792.	4.8	44
69	Facile fabrication of conductive ultrahigh molecular weight polyethylene fibers via musselâ€inspired deposition. Journal of Applied Polymer Science, 2013, 128, 1030-1035.	2.6	22
70	Electrostatic adsorption method for preparing electrically conducting ultrahigh molecular weight polyethylene/graphene nanosheets composites with a segregated network. Composites Science and Technology, 2013, 89, 180-185.	7.8	60
71	Living lamellar crystal initiating polymerization and brittleness mechanism investigations based on crystallization during the ring-opening of cyclic butylene terephthalate oligomers. Polymer Chemistry, 2013, 4, 1648.	3.9	9
72	Coupling between crystallization and evaporation dynamics: Periodically nonlinear growth into concentric ringed spherulites. Polymer, 2013, 54, 6628-6635.	3.8	16

#	Article	IF	CITATIONS
73	Solution crystallization behavior of linear and star-shaped poly(ethylene) Tj ETQq1 1 0.784314 rgBT /Overlock 10 2013, 31, 1717-1724.	Tf 50 747 3.8	Td (glycol) 8
74	Synthesis and characterization of triblock copolymer PLA-b-PBT-b-PLA and its effect on the crystallization of PLA. RSC Advances, 2013, 3, 18464.	3.6	23
75	Crystallization behavior, thermal and mechanical properties of PHBV/graphene nanosheet composites. Chinese Journal of Polymer Science (English Edition), 2013, 31, 670-678.	3.8	38
76	Noncovalent Method for Improving the Interaction between Reduced Graphene Oxide and Poly(ε-caprolactone). Industrial & Engineering Chemistry Research, 2013, 52, 15824-15828.	3.7	22
77	Crystallization and morphology of star-shaped polyethylenoxyde-b-polycaprolactone under high pressure carbon dioxide. Chinese Journal of Polymer Science (English Edition), 2012, 30, 623-631.	3.8	6
78	Band-to-Nonband Transition into Unique Poly(Îμ-caprolactone) Crystals by Modulating the Interplay of Diffusion and Growth. ACS Macro Letters, 2012, 1, 718-722.	4.8	24
79	Rhythmic Growth Combined with Lamellar Twisting Induces Poly(ethylene adipate) Nested Ring-Banded Structures. ACS Macro Letters, 2012, 1, 154-158.	4.8	39
80	Chitin nanocrystals grafted with poly(3-hydroxybutyrate-co-3-hydroxyvalerate) and their effects on thermal behavior of PHBV. Carbohydrate Polymers, 2012, 87, 784-789.	10.2	65
81	Twisting of Lamellar Crystals in Poly(3-hydroxybutyrate- <i>co</i> -3-hydroxyvalerate) Ring-Banded Spherulites. Macromolecules, 2010, 43, 4441-4444.	4.8	58
82	Rhythmic Growth-Induced Ring-Banded Spherulites with Radial Periodic Variation of Thicknesses Grown from Poly(Îμ-caprolactone) Solution with Constant Concentration. Macromolecules, 2008, 41, 7584-7595.	4.8	81
83	Rhythmic Growth-Induced Concentric Ring-Banded Structures in Poly(ε-caprolactone) Solution-Casting Films Obtained at the Slow Solvent Evaporation Rate. Macromolecules, 2007, 40, 4381-4385.	4.8	68